Pergamon

Cement and Concrete Research 30 (2000) 791–798

CEMENT AND CONCRETE RESEARCH

Cracking tendency of alkali-activated slag concrete subjected to restrained shrinkage

Frank Collins[a,*], J.G. Sanjayan[b]

[a]*Maunsell McIntyre Pty Ltd, Level 9, 161 Collins Street, Melbourne, Victoria 3000, Australia*
[b]*Department of Civil Engineering, Monash University, Clayton, Victoria 3168, Australia*

Received 20 September 1999; accepted 22 February 2000

Abstract

Alkali-activated slag concrete (AASC) has higher drying shrinkage than ordinary Portland cement concrete (OPCC). However, the cracking tendency of AASC under drying conditions, when restrained, is unreported. AASC has lower elastic modulus, higher creep, and higher tensile strength than OPCC, and the combined effects of these can affect the cracking tendency of AASC. This article reports the results of cracking tendency utilizing restrained ring tests and discusses the development of a restrained beam test. The effects of curing, aggregate type, and incorporation of shrinkage reducing chemical admixture on the cracking tendency of AASC are reported.

Keywords: Granulated blast furnace slag; Alkali-activated cement; Curing; Shrinkage; Crack detection

1. Introduction

Drying shrinkage of alkali-activated slag concrete (AASC) can be 1.6 to 2.1 times greater than ordinary Portland cement (OPC) mortar and concrete [1–11]. The high drying shrinkage of AASC, which translates into a greater cracking tendency than ordinary Portland cement concrete (OPCC), is not reported in the literature. The magnitude of drying shrinkage that is measured on small prisms does not necessarily relate to the cracking tendency when a structural member is restrained. When comparing AASC and OPCC, it is difficult to discern the cracking risk due to significantly different shrinkage, creep, elastic modulus, and tensile strength properties of the two concretes. This investigation sought to assess cracking tendency of AASC and study the effects of curing, replacement of normal weight coarse aggregate with BFS aggregate, and use of shrinkage reducing chemical admixture.

2. Experimental program

The chemical composition and properties of the cementitious binders are summarized in Table 1.

The binders used are ground granulated blast furnace slag (Slag) and OPC. The term water/binder (w/b) ratio is used instead of water/cement ratio (w/c) to refer to both the binders mentioned above. The slag is supplied with gypsum (2% SO_3), which is blended with the slag. The activators and adjuncts utilized were powdered sodium metasilicate and hydrated lime and the method of use in concrete has been outlined earlier by Collins and Sanjayan [9].

The normal weight aggregates consisted of 14 mm maximum size basalt and river sand. Air-cooled blast furnace slag was also used as coarse aggregate. The properties of the aggregates, proportioning, and method of pre-saturation have been described previously by Collins and Sanjayan [12].

The concrete mixture proportions are summarized in Table 2. Allowance for moisture content in the aggregates (based on saturated and surface dry conditions), powdered sodium silicate activator, and hydrated lime slurry was made to ensure correct free water content in the mixture.

* Corresponding author. Tel.: +61-3-9653-1234; fax: +61-3-9654-7117.
E-mail address: fgco@maunsell.com.au (F. Collins).

0008-8846/00/$ – see front matter
PII: S0008-8846(00)00243-X

3. Unrestrained shrinkage

Shrinkage prisms (75 × 75 × 285 mm) were made in accordance with Australian Standard AS1012.13. The prisms were made in triplicate sets and sealed at 23°C for 24 h followed by exposure to 23°C temperature and 50% relative humidity (RH).

Fig. 1 shows similar magnitude of drying shrinkage of concrete mixtures OPCC, AASC/SR, AASC/BFS at 56 days although AASC/BFS has significantly lower early age drying shrinkage. At 56 days, AASC shows 1.6 times greater drying shrinkage than OPCC.

Table 2
Summary of concrete mixture proportions (kg/m^3)

Constituents	OPCC	AASC	AASC/SR[a]	AASC/BFS
OPC	360	180	180	–
Slag	–	180	180	360
Free water	180	180	180	180
w/b	0.5	0.5	0.5	0.5
Fine aggregate	830	830	830	830
Basalt coarse aggregate 14 mm	1130	1130	1130	–
BFS coarse aggregate 14 mm	–	–	–	990
Air content (%)	0.5	1.2	1.6	1.6

[a] AASC/SR contained 1.5% shrinkage reducing chemical admixture, *Eclipse*™.

4. Restrained ring

Three identical restrained rings consisting of mixture types OPCC and AASC (i.e. six numbers total) were made. The dimensions of the restrained ring specimens used in this investigation are shown in Fig. 2. The sample geometry is very similar to those of Folliard and Berke [13]. The inner restraining ring consisted of a steel hollow bar that had an outside diameter of 298 mm and an inside diameter of 248 mm and was cut to a length of 150 mm. The concrete was placed within an annulus bounded by a PVC pipe with an internal diameter of 382 mm and the steel internal restraining ring. Following concrete placement and finishing, the rings were covered with impervious polythene sheet to prevent air circulation at 23°C temperature for 24 h prior to removal from the mould. The top and bottom surfaces were sealed and the sample was stored at 50% RH and 23°C temperature. The crack width was measured at the widest location on a crack with a crack detection microscope that had 0.01-mm divisions, 40× magnification, and a built-in light source. The crack area is defined as the product of crack width multiplied by crack length, a parameter used, for example, by Collins and Roper [14]. For a given concrete ring, the sum of the crack areas was calculated and for a data set of three rings, the average crack area was calculated.

The OPCC restrained rings cracked 168 days from the time of exposure to 50% RH and 23°C temperature. The cracks were ery fine, ranging in width from 0.02 to 0.06 mm. The crack areas for the three restrained rings were 9.62, 6.1, and 2.12 mm^2, which is considered to be highly variable. The AASC restrained rings cracked 7 days from the time of exposure to 50% RH and 23°C. The progressive increase in crack area from the time of first cracking to 168 days from the time of exposure is shown in Fig. 3. The growth of crack area with time is rapid from 7 to 21 days and reaches a limit virtually from 91 days onwards. The crack area shown is the mean crack area of the three samples tested. The crack areas for three restrained rings within a data set are quite variable and the ratio of the sample range of crack areas to sample mean of crack areas was 0.9.

Table 1
Properties of cementitious materials

Constituent/property	Slag	OPC
SiO_2 (%)	35.04	19.9
Al_2O_3 (%)	13.91	4.62
Fe_2O_3 (%)	0.29	3.97
MgO (%)	6.13	1.73
CaO (%)	39.43	64.27
Na_2O (%)	0.34	–
TiO_2 (%)	0.42	–
K_2O (%)	0.39	0.57
P_2O_5 (%)	<0.1	–
MnO (%)	0.43	–
Total sulfur as SO_3 (%)	2.43	2.56
Sulfur as S^{2-}	0.44	–
Cl (ppm)	80	–
Fineness (m^2/kg)	460	342
Loss on ignition (%)	1.45	2.9
Time to initial set (h)	N/A	2.0
Strength of 70 × 70 × 70 mm mortar cubes (MPa)		
3 days	N/A	32.7
7 days		42.0
28 days		54.1

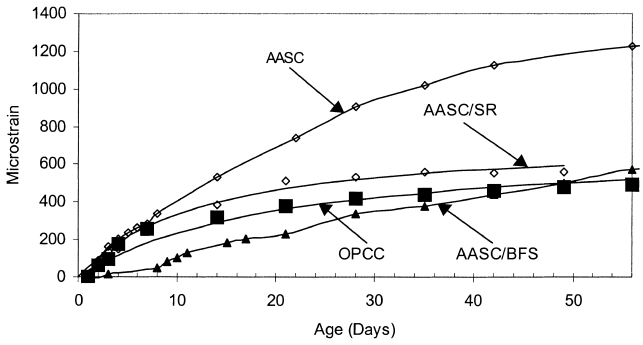

Fig. 1. Drying shrinkage of concrete prisms subject to sealed curing at 23°C temperature for 24 h followed by exposure to 23°C temperature and 50% RH.

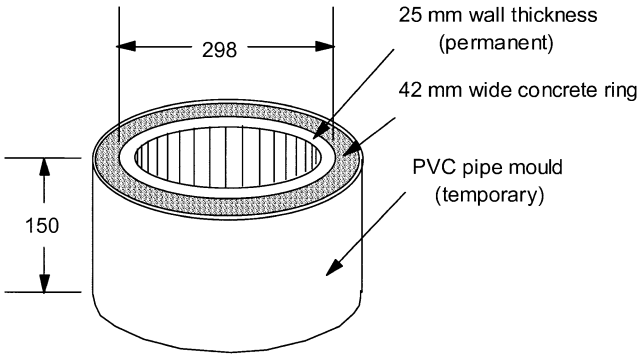

Fig. 2. Experimental set-up for the restrained ring test.

Although the restrained ring test differentiates the different cracking tendency of OPCC and AASC, use of the test to compare AASC/SR and AASC/BFS was discontinued for the following reasons:

1. The lengthy period of time taken for cracking in OPCC to commence;
2. The small crack width of OPCC restrained rings made crack detection difficult;
3. The recording of crack length and width was tedious given the random locations of the cracks;
4. The specimen is subject to differential drying (i.e. a humidity gradient is set up between the inside face, which is restrained, and the outer circumferential surface, which is exposed);
5. In some cases, the restrained ring test does not lead to cracking [13,15–17]. It is difficult to rank the relative crack tendency between concrete types that show no cracking.

An alternative test was therefore developed that showed greater sensitivity to cracking and overcame the need to conduct tedious measurement of randomly distributed cracks.

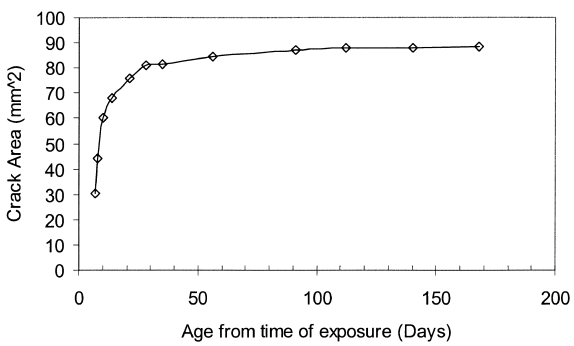

Fig. 3. Crack area vs. time for AASC restrained rings.

5. Development of a restrained beam test

5.1. Test configuration

One of the advantages of using a restrained beam test is that similar sample dimensions of the beam could be used to the prisms utilized for testing of unrestrained shrinkage to the Australian Standard AS1012.13. The restrained beams used in this investigation were therefore modeled on a similar type of beam reported by Roper [18] and the dimensions were 75-mm width, 150-mm depth, and 1000-mm length. The experimental set-up of the restrained beam test incorporating two steel rods is shown in Fig. 4.

Internal restraint is provided by 25-mm diameter round mild steel rods, which were cast into the beam. The central 600-mm portion of the rod was machined smooth to minimize concrete-to-steel bond and had a layer of grease applied to the surface while the 200-mm portions at each end were machined with a coarse thread to provide bond and hence, anchorage. Two nuts were placed along the threaded portions of rod to assist with anchorage. A third nut at each end provides support to the end formwork. The top of the moulded concrete was made level and smooth by trowel and was immediately covered with impervious polythene sheet to prevent air circulation over the placed concrete. The samples were stored at 23°C temperature for 24 h prior to removal of the concrete beams from the mould. Following demoulding, the beams were placed on roller supports (positioned at mid-span and at each end) and exposed to 50% RH and 23°C temperature.

5.2. Effect of the number of embedded greased rods

The effects of the number of embedded rods, and hence, the effects of restraint, were initially investigated. A total of

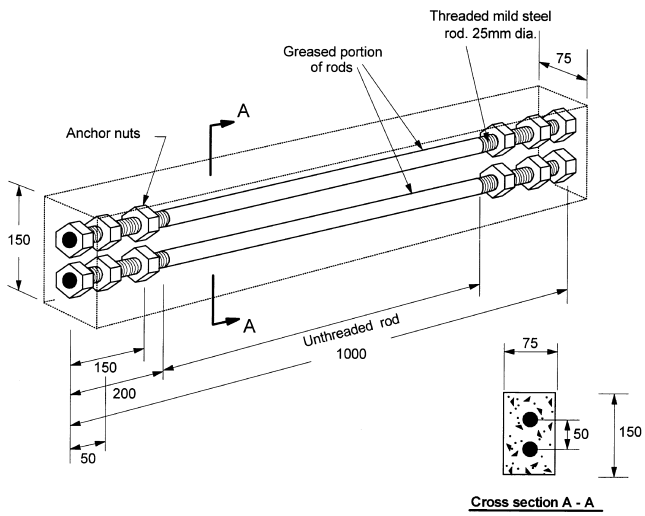

Fig. 4. Typical experimental set-up for the restrained beam test.

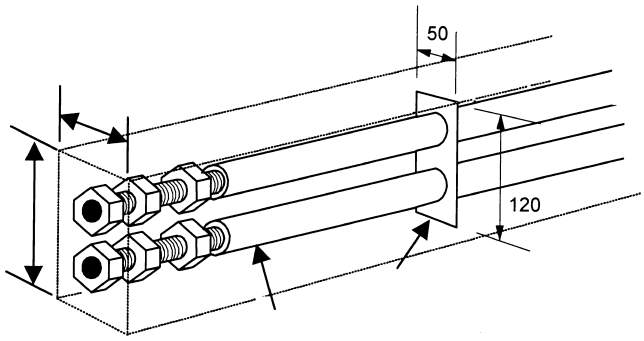

Fig. 5. Position of stress magnifier plate.

six beams (three of AASC and three of OPCC), were cast. Each of the three beams for a concrete type contained one, two, or three 25-mm diameter mild steel rods, respectively, which were positioned centrally along the vertical axis and are equidistant from each other. The steel rods had surface grease applied to break the concrete-to-rod bond.

After 120 days of curing, none of the six beams cracked, irrespective of the concrete type or the amount of internal restraint. It is concluded that the beams did not crack because of inadequate de-bonding of the central portions of the rods to the concrete. It was decided to repeat the test and to eliminate the rod-to-concrete bond by providing sheathing to the rods.

5.3. Effect of the number of embedded sheathed rods

To eliminate concrete-to-steel rod bond, thin, non-rigid PVC electrical insulation sheathing with 26-mm internal diameter was fitted over each rod. The ends of the sheathing were sealed with PVC adhesive duct tape to prevent seepage of cementitious paste from the concrete between the sheath and the rod.

A total of six beams (three of AASC and three of OPCC) were made. The method of testing is the same as described above. Restrained beams that contained two embedded rods showed visible cracks at 21 days for OPCC and at 5 days for AASC. The cracks occurred within the region of the sheathed length of steel rod; however, the location of the cracks was at random along the length of the beam. The AASC restrained beams displayed visible surface crazing, and this may have contributed to the crack propagation.

Cracking was not observed in the beams with one embedded rod. This could be most likely due to insufficient restraint being generated to cause cracking. Both OPCC and AASC beams containing three embedded rods were also uncracked. This is difficult to explain. One possible explanation is that with three rods configuration, minor misalignments of the bars during concrete placement could have restricted movement of the concrete along the sheathed length of bar thus preventing cracking. Further, it was decided that the three-bar arrangement caused congestion, thus making concrete placement and compaction within the beam difficult. It was decided to adopt two embedded rods for further experimentation and to develop means of confining the induced crack to one location in the beam to enable repeatable measurements of crack width to be conducted.

5.4. Effect of embedded stress magnifier plate

A thin, mild steel stress magnifier plate was cast into the center of the beam, as shown in Fig. 5. The purpose of the plate was to generate the crack at the center of the beam. Furthermore, the level of tensile stress generated within the concrete could be adjusted simply by altering the size of the plate and thus changing the area of concrete subject to tensile stress at the plate location. The dimensions of the plate used in this investigation were $50 \times 120 \times 2$ mm, with holes drilled to accommodate the two sheathed restraining rods. To prevent plate-to-concrete bond, the stress magnifier plates were wrapped with layers of thin PVC film prior to installation within the mould.

A total of six restrained beams containing two embedded and sheathed bars were cast (three OPCC and three AASC). The beams were made and tested using the same procedures as described above. The crack width was measured at the top and side at the widest location with a crack detection microscope.

Following exposure to 50% RH and 23°C temperature, all three OPCC beams cracked around the perimeter of the beam at the plate location on the 9th day. The initial crack width was 0.09 mm and the crack grew to a width of 0.33 mm at 175 days from the time of first cracking. The crack width development with time is shown in Fig. 6. Each data set is the mean of all crack width measurements on each of the three beams. Following exposure to 50% RH and 23°C temperature, one AASC beam cracked within 7 h and the other two beams between 7 and 24 h. The crack was found around the perimeter of the beam at the stress magnifier plate location, which was positioned at the center of the beam. The crack grew rapidly from 0.12 mm at about the time of cracking to 0.97 mm at 175 days from the day of first cracking. The crack width development with time is shown in Fig. 6.

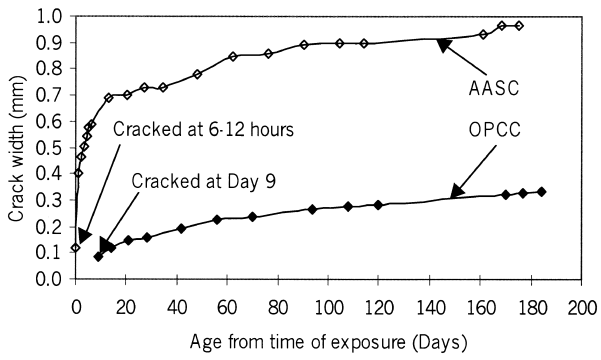

Fig. 6. OPCC and AASC exposed from day 1.

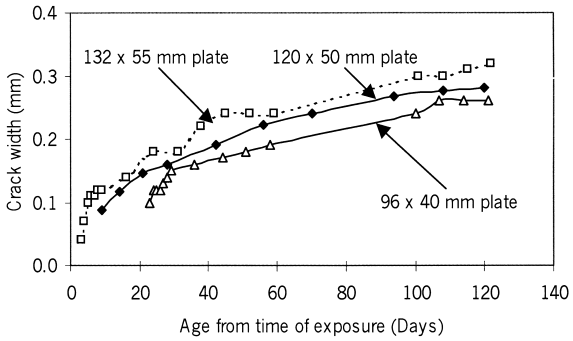

Fig. 7. Effect of size of stress magnifier plate (OPCC restrained beams).

Each of the three identical beams in each data set cracked within the same day and the stress magnifier plate produced a consistent crack around the perimeter of the beam that had good definition for measurement purposes.

5.5. Effect of stress magnifier plate size

The size of the stress magnifier plate that was cast into the beams was 50 × 120 mm. Two additional OPCC beams were made to assess the effect of plate size on the time to cracking. The sizes of the plates in these beams were 40× 96 and 55 × 132 mm. The crack development with time is shown in Fig. 7.

The time to cracking from the day of exposure for the beams, in order of ascending plate size, was 23, 9, and 3 days. At the time of cracking, the size of the crack is smaller with increasing size of plate. However, at later ages, the width of the crack is greater with increasing size of the plate.

The size of the plate affects the time of cracking, as shown in Table 3. Cracks initiated by all the plates are similar at the time of cracking and approach the same crack width with time. This agrees well with the theory that the plates are stress magnifiers and therefore only affects the time to cracking, whereas the crack widths are a function of shrinkage only.

The medium-sized plate (i.e. 50 × 120 mm) was selected for further beam experiments since it provides good definition of time to cracking when ranking the two different types of concrete, AASC and OPCC (9 days time to cracking for OPCC vs. 1 day time to cracking for AASC).

Table 3
Summary of time to cracking and crack width for different stress magnifier plate sizes

Plate size (mm)	Time to cracking (days)	Crack width at time of cracking (mm)	Crack width at 100 days from time of cracking (mm)
132 × 55	3	0.11	0.30
120 × 50 (three beams)	9	0.09	0.28
96 × 40	23	0.10	0.26

For other types of concrete with different drying shrinkage characteristics to OPCC and AASC, incorporation of different stress magnifier plate sizes would enable more versatile use of the test to assess different concrete types with either low or high drying shrinkage.

6. Effect of bath curing

Bath curing permits tensile strength to develop and could increase the length of time to cracking. Also, it is likely that the surface crazing/microcracking, which is visible on the surface of AASC when exposed from day 1, could serve as crack initiator thus leading to propagation of major shrinkage cracks.

Two AASC beams were made and, 1 day after concrete placement and following formwork removal, were bath-cured in lime-saturated water at 23°C for 3 and 14 days, then subjected to 50% RH and 23°C exposure. The progression of cracking is summarized in Fig. 8.

Following removal from the bath, the 3- and 14-day bath-cured AASC beams cracked at 2 and 25 days, respectively following exposure to 50% RH and 23°C temperature. The bath-cured beams show considerably lower crack width than AASC with no prior bath curing. This emphasizes the critical importance of the need for good curing of AASC.

An OPCC beam was made and 1 day after concrete placement and following formwork removal, the beam was bath-cured in lime-saturated water at 23°C for 3 days, then exposed to 50% RH and 23°C temperature. The progression of cracking is summarized in Fig. 9. The bath-cured beam cracked 16 days following exposure to 50% RH and 23°C temperature. The magnitude of crack width with time is similar to the OPCC beams that were exposed from day 1 onwards. Although the 3-day bath-cured AASC beam cracked within 2 days, the magnitude of crack width with time is similar to OPCC bath-cured for 3 days. Following the trends shown in Fig. 8, which indicate lower crack width of AASC beams with increasing time of initial bath curing,

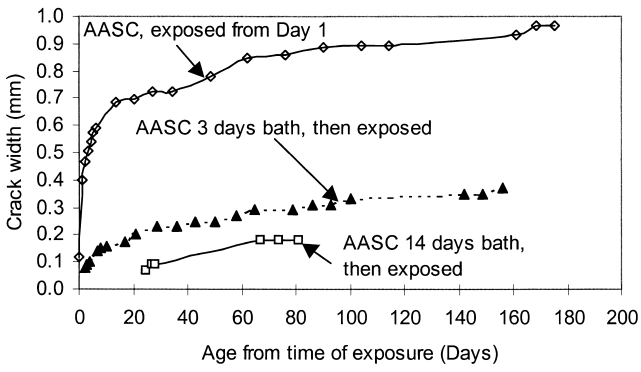

Fig. 8. Effect of bath curing on AASC beams.

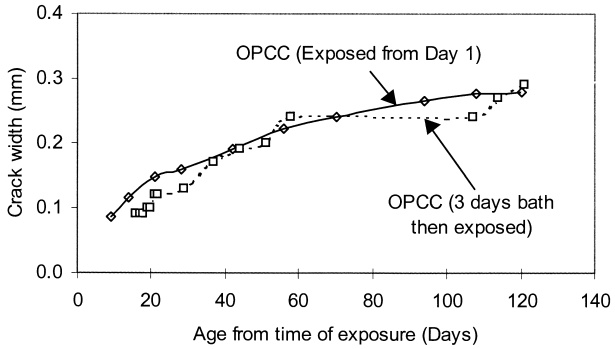

Fig. 9. Effect of bath curing on OPCC beams.

Fig. 9 would be expected to show the same trend. Longer duration of initial bath curing of OPCC beams was not undertaken in this investigation.

7. Effect of shrinkage reducing chemical admixture

Three restrained beams were made which were based on the AASC/SR. The beams were subjected to 0, 3, and 7 days bath curing in lime-saturated water at 23°C temperature prior to exposure to 50% RH and 23°C temperature. The crack development with age is shown in Fig. 10.

The beam that was exposed from day 1 cracked within 1 day. However, the width of the crack that was generated was 37.7% less than AASC beams at 141 days due to the reduced amount of drying shrinkage in the mixture AASC/SR. Although AASC/SR has lower magnitude of drying shrinkage than AASC, the early age compressive strength is lower [19] and the implied tensile strength difference may explain similar time to cracking. Bath curing delayed the time to cracking to 3 and 6 days from the time of exposure for the 3- and 7-day bath-cured beams, respectively. However, the width of the cracks has been significantly reduced to values comparable to OPCC for 3-day bath-cured AASC/SR beams and less than OPCC for 7-day bath-cured PSS/SR beams. It should be noted that the 3-day bath-cured AASC beam shows almost identical time to cracking and crack width at 56 days from the time to cracking to AASC/SR, which was also bath-cured initially for 3 days. Therefore, inclusion of a shrinkage reducing chemical admixture has little effect on AASC beams provided that adequate bath curing is provided.

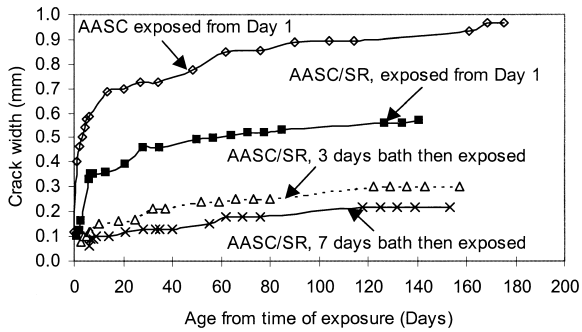

Fig. 10. Effect of shrinkage reducing chemical admixture and curing on AASC.

8. Effect of BFS aggregate

As shown by Collins and Sanjayan [12], replacement of normal weight coarse aggregate with BFS coarse aggregate into AASC significantly reduces the magnitude of drying shrinkage.

Three restrained beams of AASC/BFS were subjected to 0, 3, and 7 days bath curing in lime-saturated water at 23°C temperature prior to exposure to 50% RH and 23°C temperature. The crack development with time is shown in Fig. 11.

A fine crack was measured 10 days from the time of exposure to 50% RH and 23°C temperature on the beam, which was exposed from the time of formwork removal (i.e. at day 1). The crack width growth in this beam was less than OPCC beams that were exposed from day 1 onwards. Following the elapse of 175 days from the time of removal from the bath and exposure to 50% RH and 23°C temperature, the 3- and 7-day bath-cured beams were not cracked.

The superior performance of the AASC/BFS beams to the AASC beams could be due to a number of reasons. Firstly, AASC/BFS has considerably lower magnitude of drying shrinkage. Secondly, AASC/BFS shows superior compressive strength, as was shown by Collins and Sanjayan [12] and the implied superior tensile strength would reduce the cracking tendency. Thirdly, Haque et al. [20] have shown the elastic modulus of OPCC incorporating BFS coarse aggregate to be lower than the same concrete mixture that incorporated normal weight coarse aggregate. Lower stiffness of AASC/BFS could explain why this concrete type accommodates more strain before cracking. Finally, AASC/BFS shows no surface microcracking in contrast with PSS beams that were exposed from day 1 onwards. The absence of crazing eliminates the possibility

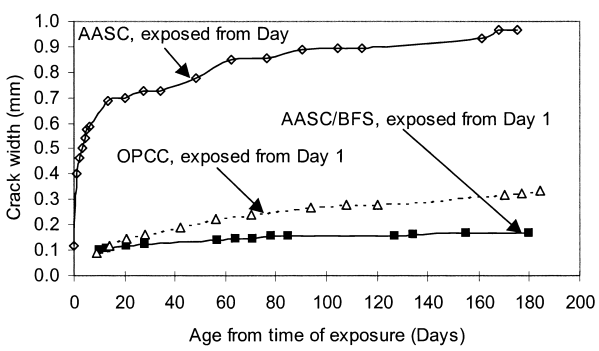

Fig. 11. Effect of BFS coarse aggregate on AASC.

of these types of cracks serving as initiators of drying shrinkage cracks.

9. Conclusions

Drying shrinkage testing according to standards (e.g. Australian Standard AS1012.13, 1992) involves measurement of free shrinkage of concrete prisms. However, this does not verify whether, under restrained conditions, a particular concrete type has greater cracking tendency. When comparing AASC with other concrete types, it is difficult to discern the relative cracking tendency due to different creep, elastic modulus, and tensile strength.

Restrained ring tests were conducted to determine cracking tendency. The test results showed considerable variation within a data set of three samples. Further, the time for OPCC restrained rings to crack was considered to be too lengthy (168 days) for practical consideration. The regular recording of the dimensions of randomly distributed cracks was also considered to be tedious.

A restrained beam test has been developed, which overcomes the above-mentioned difficulties with restrained ring tests, and further has the advantage that the width of the beam is identical to the prism width of unrestrained shrinkage test specimens made to the Australian standard. The key outcomes from the restrained beam test are as follows:

(i) Following demoulding at day 1, AASC beams that were exposed to 50% RH and 23°C temperature cracked within 1 day and grew to 0.97 mm at 175 days, whereas OPCC beams cracked within 9 days and grew to a width of 0.33 mm at 175 days.

(ii) AASC beams that were bath-cured in lime-saturated water for 3 and 14 days prior to exposure to 50% RH and 23°C temperature cracked respectively at 2 and 44 days after exposure; however, the magnitude of the crack width was considerably less than AASC beams which had no curing. The crack width was comparable to the OPCC restrained beams. Attention to good curing is therefore essential when utilizing AASC concrete.

(iii) Incorporation of shrinkage reducing chemical admixture, SR, did not delay the time to cracking of AASC exposed from day 1. However, the crack width was considerably reduced and was slightly greater than OPCC that was exposed from day 1. Although AASC/SR has lower magnitude of drying shrinkage than AASC, the early age compressive strength is lower [19] and the implied tensile strength difference may explain similar time to cracking. Bath curing of AASC/SR beams for 3 and 7 days delayed the onset of cracking to 3 and 6 days, respectively. The width of the cracks has been significantly reduced to values comparable to OPCC for 3-day bath-cured AASC/SR beams and less than OPCC for 7-day bath-cured AASC/SR beams. The 3-day bath-cured AASC beam shows almost identical time to cracking and crack width at 56 days from the time to cracking to AASC/SR, which was also bath-cured initially for 3 days. Therefore, inclusion of a shrinkage reducing chemical admixture has little effect on AASC beams when adequate bath curing is provided.

(iv) AASC/BFS demonstrated the best cracking tendency performance of all the restrained beams. A fine crack was measured 10 days from the time of exposure to 50% RH and 23°C temperature on the beam, which was exposed from day 1. The crack width growth was less than OPCC beams that were exposed from day 1 onwards. Following the elapse of 175 days from the time of removal from the bath and exposure to 50% RH and 23°C temperature, the 3- and 7-day bath-cured beams were uncracked.

The superior performance of the AASC/BFS beams could be due to lower magnitude of drying shrinkage, superior tensile strength, and lower elastic modulus than AASC with normal weight coarse aggregate. Lower stiffness of AASC/BFS could explain why this concrete type accommodates more strain before cracking. AASC/BFS shows no surface crazing in contrast with AASC when exposed from day 1 onwards. The absence of crazing eliminates the possibility of these types of cracks serving as initiators of drying shrinkage cracks. AASC/BFS and AASC/SR show similar magnitude of drying shrinkage; however, the two concrete types have different cracking tendency.

Acknowledgments

The financial support for this project is jointly provided by Independent Cement and Lime, Blue Circle Southern Cement, and Australian Steel Mill Services. The authors thank the sponsors especially Alan Dow, Tom Wauer, Katherine Turner, Wayne James, Paul Ratcliff, John Ashby, and Dr. Ihor Hinczak for the guidance and support. The enthusiastic participation of final year students Lee Tuan Kuan and Eric Tan in this project is very much appreciated. The efforts and assistance with the laboratory work provided by Jeff Doddrell, Roger Doulis, and Peter Dunbar are also gratefully acknowledged.

References

[1] T. Kutti, L. Berntsson, S. Chandra, Shrinkage of cements with high content of blast-furnace slag, Proc. Fourth CANMET/ACI International Conference on Fly Ash, Silica Fume, Slag, and Natural Pozzolans in Concrete, Istanbul, Turkey (3) (1992) 615–625.

[2] J. Malolepszy, J. Deja, The influence of curing conditions on the mechanical properties of alkali activated slag binders, Silic Ind 11 (12) (1988) 179–186.

[3] T. Hakkinen, The microstructure of high strength blast furnace slag concrete, Nord Concr Res 11 (1992) 67–82.

[4] E. Douglas, A. Bilodeau, V.M. Malhotra, Properties and durability of alkali-activated slag concrete, ACI Mater J 89 (5) (1992) 509–516.

[5] T. Hakkinen, Properties of alkali-activated slag concrete, Tech Res Cent Finl Res Notes 540 (1986) 1–62.
[6] H. Kukko, R. Mannonen, Chemical and mechanical properties of alkali-activated blast furnace slag (F-concrete), Nord Concr Res 1 (1982) 16.1–16.16.
[7] W. Jiang, M.R. Silsbee, D.M. Roy, Alkali activation reaction mechanism and its influences on microstructure of slag cement, Proc. 10th ICCC (3) (ii) (100) (1997) 1–9.
[8] R. Andersson, H.E. Gram, Properties of alkali-activated slag, in: R. Andersson, H.E. Gram, J. Malolepszy, J. Deja (Eds.), Alkali-Activated Slag, Swed Cem Concr Inst Rep, vol. 1.88, 1988, pp. 9–65.
[9] F.G. Collins, J.G. Sanjayan, Workability and mechanical properties of alkali activated slag concrete, Cem Concr Res 29 (3) (1999) 455–458.
[10] T. Kutti, Hydration products of alkali-activated slag, Proc. 9th ICCC, New Delhi, India 4, (1992) 468–474.
[11] S.D. Wang, Alkaline activation of slag, Ph.D. dissertation, Imperial College of Science, Technology and Medicine, University of London, 1995.
[12] F.G. Collins, J.G. Sanjayan, Strength and shrinkage properties of alkali activated slag concrete containing porous coarse aggregate, Cem Concr Res 29 (4) (1999) 607–610.
[13] K.J. Folliard, N.S. Berke, Properties of high-performance concrete containing shrinkage-reducing admixture, Cem Concr Res 27 (9) (1997) 1357–1364.
[14] F.G. Collins, H. Roper, Laboratory investigation of shear repair of reinforced concrete beams loaded in flexure, ACI Mater J 97 (2) (1990) 149–159.
[15] R.N. Swamy, H. Stavrides, Influence of fibre reinforcement on restrained shrinkage and cracking, ACI J (3) (1979) 443–460.
[16] H. Krenchel, S. Shah, Restrained shrinkage tests with PP-fibre reinforced concrete, in: S.P. Shah, G.B. Batson (Eds.), Proc. Fibre Reinforced Concrete Properties and Applications, ACI SP-105, vol 1, 1987, pp. 141–158.
[17] S.P. Shah, C. Ouyang, S. Marikunte, W. Yang, E. Becq-Giraudonb, A method to predict shrinkage cracking of concrete, ACI Mater J 95 (4) (1998) 339–346.
[18] H. Roper, The properties of concrete manufactured with some coarse aggregates of the Sydney area, Aust Road Res 5 (6) (1974) 40–50.
[19] F.G. Collins, High early strength concrete using alkali activated slag, Ph.D. dissertation, Department of Civil Engineering, Monash University, 1999.
[20] M.N. Haque, O.A. Kayyali, B.M. Joynes, Blast furnace slag aggregate in the production of high performance concrete, in: V.M. Malhotra (Ed.), Proc. 5th CANMET/ACI International Conference on Fly Ash, Silica Fume, Slag, and Natural Pozzolans in Concrete, Milwaukee, USA, ACI SP-153, vol. 2, 1995, pp. 911–930.